Check for updates

ChemMedChem

Research Article
doi.org/10.1002/cmdc.202200647

Chemistry Europe
European Chemical Societies Publishing

www.chemmedchem.org

Development of Light-Activated LXR Agonists

Tufan K. Mukhopadhyay[+],[b] Sabine Willems[+],[c] Christopher J. Arp,[b] Johannes Morstein,[b] Caleb T. Haake,[b] Daniel Merk,*[c] and Dirk Trauner*[a]

Activation of the oxysterol-sensing transcription factor liver X receptor (LXR) has been studied as a therapeutic strategy in metabolic diseases and cancer but is compromised by the side effects of LXR agonists. Local LXR activation in cancer treatment may offer an opportunity to overcome this issue suggesting potential uses of photopharmacology. We report the computer-aided development of photoswitchable LXR agonists based on the T0901317 scaffold, which is a known LXR agonist. Azologization and structure-guided structure-activity relationship evaluation enabled the design of an LXR agonist, which activated LXR with low micromolar potency in its light-induced (*Z*)-state and was inactive as (*E*)-isomer. This tool sensitized human lung cancer cells to chemotherapeutic treatment in a light-dependent manner supporting potential of locally activated LXR agonists as adjuvant cancer treatment.

Introduction

The liver X receptors (LXRs) are ligand-activated transcription factors of the nuclear hormone receptor type. They exist in two isoforms, LXRα (NR1H3) and LXRβ (NR1H2), which share a high sequence identity (78% in the ligand binding domain, LBD).[1,2] LXRα is mainly found in the liver, intestine, adipose tissue, and macrophages, while LXRβ occurs ubiquitously.[2] Both receptors act as cellular sensors of oxidized cholesterol derivatives, oxysterols, such as 24(*S*)-hydroxycholesterol (**1**, Scheme 1), highlighting their role as key regulators of cholesterol homeostasis.[1,3,4] LXRs control the peripheral uptake of cholesterol, its transport, and excretion into the liver by regulating the expression of cholesterol transporter proteins named ATP-binding cassette transporter A1 and G1 (ABCA1 and ABCG1) as well as the apolipoproteins ApoE and ApoC.[1,3] With concomitant anti-inflammatory effects of LXR activation, this physiological role has rendered LXRs promising targets to treat metabolic and cardiovascular diseases.[5]

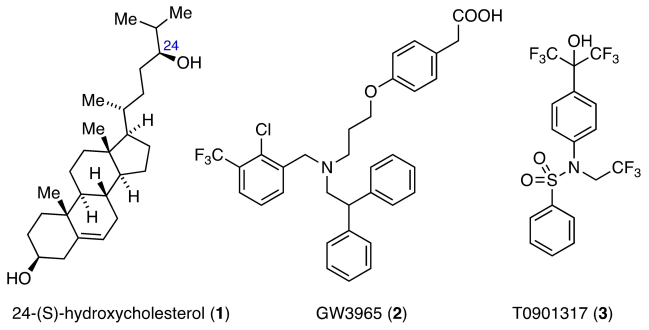

24-(S)-hydroxycholesterol (**1**) GW3965 (**2**) T0901317 (**3**)

Scheme 1. LXR agonists.

Several potent synthetic LXR agonists have been developed as chemical tools and experimental drugs to capture the therapeutic potential of LXR activation. Among them, GW3965 (**2**)[6] and T0901317 (**3**)[7] (Scheme 1) are widely used reference agonists that are equally active on both LXR isoforms. However, enhanced hepatic lipogenesis as a side effect of LXRα activation has impeded the therapeutic use of LXR agonists in metabolic diseases.[7] Recent findings support additional pharmacological potential of LXR activation in certain types of cancer and in neurodegenerative diseases, which remains to be clinically validated.[8–10]

Photopharmacology enables the optical control of biological processes with high spatiotemporal precision by using photoswitchable molecules that exhibit different activity in their different configurations.[11–14] This concept has been established for several protein classes, including nuclear receptors,[15–20] and is also appealing for LXR activation as it may reduce systemic side effects through local activation.[21] Especially for an application in cancer treatment, this approach holds potential by spatially limiting pharmacological effects to an intended site of action.[21] Here we report the development of light activated LXR agonists from the template T0901317 (**3**), which was supported by molecular docking studies. Azobenzene, whose diazene (-N=N-) unit is an isostere of the

[a] *Prof. D. Trauner*
Department of Chemistry
University of Pennsylvania
College of Arts and Sciences
231 South 34th Street, Philadelphia, PA 19104-6323 (USA)
E-mail: dtrauner@upenn.edu
[b] *Dr. T. K. Mukhopadhyay,[+] C. J. Arp, Dr. J. Morstein, C. T. Haake*
Department of Chemistry
New York University
New York City, NY 10003 (USA)
[c] *Dr. S. Willems,[+] Prof. D. Merk*
Department of Pharmacy
Ludwig-Maximilians-Universität München
Butenandtstraße 5–13, 81377 Munich (Germany)
E-mail: daniel.merk@cup.lmu.de
[+] *These authors contributed equally to this work.*

Supporting information for this article is available on the WWW under https://doi.org/10.1002/cmdc.202200647

© 2023 The Authors. ChemMedChem published by Wiley-VCH GmbH. This is an open access article under the terms of the Creative Commons Attribution Non-Commercial NoDerivs License, which permits use and distribution in any medium, provided the original work is properly cited, the use is non-commercial and no modifications or adaptations are made.

© 2023 The Authors. ChemMedChem published by Wiley-VCH GmbH

sulphonamide linker group of **3**, [15] was used to achieve photoisomerization. Computer-aided optimization of the initial T0901317 azolog **4** resulted in compound **14**, which exhibited LXR agonism only in its light-activated (*Z*)-state. Treatment of human lung cancer cells (A549) with **14** resulted in light-dependent sensitization to the apoptosis-inducer gefitinib indicating that the concept of photopharmacology may have value in cancer treatment.

Results and Discussion

Among the known LXR agonist scaffolds for which co-crystal structures were available as basis for structure-guided design, the T0901317 (**3**) chemotype seemed most amenable for the development of photoswitchable chemical tools. We envisioned to incorporate a diazene isostere in this skeleton by replacing the sulphonamide linker. Molecular docking of the basic azolog **4** of T0901317 (Figure 1a) indicated a binding mode aligning with the lead and supported our approach. Due to the spatial and conformational flexibility of the LXR ligand binding site, docking suggested favourable binding of both the (*E*)- and (*Z*)-isomers of **4** (Figure 1b). The docking results thus indicated a need for structural optimization to obtain activity differences between the isomers, which led us to further optimize the structure of **4** for preferential binding of the light-activated (*Z*)-form. In the dark, azobenzene exists as the thermodynamically favoured (*E*)-isomer (Figure 1c).

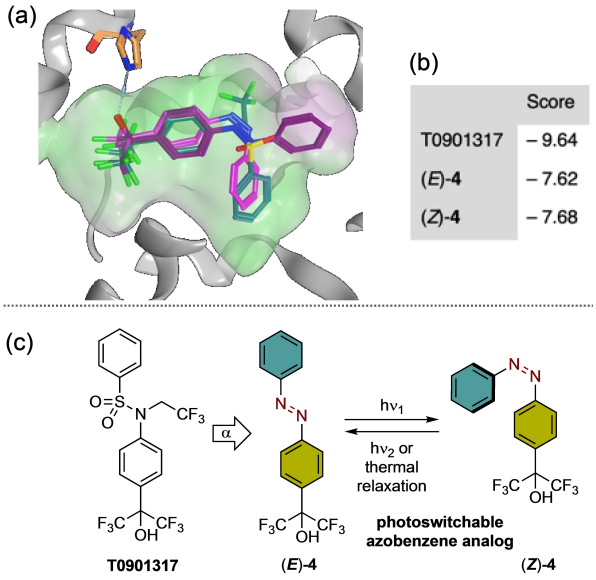

Figure 1. Design of photoactivatable LXR agonists from T0901317. (a) Docking of the T0901317 azolog **4** to the T0901317-bound LXRβ ligand binding domain (LBD) (pdb ID 1pqc)[22] indicated favourable binding of the (*E*)- and (*Z*)-isomer. Unoccupied space around the unsubstituted phenyl motif in the predicted binding mode of (*Z*)-**4** but not (*E*)-**4** suggested modifications in this region as potential avenue to analogues with (*Z*)-preferential activity on LXR. T0901317: petrol; (*E*)-**4**: purple; (*Z*)-**4**: pink. (b) Median scores for the ten top-scoring docking poses of T0901317, (*E*)-**4**, and (*Z*)-**4**. (c) Azolog design by replacing the sulphonamide with diazine linker and photoswitching phenomenon of azobenzene.

Stronger activity of the light-activated (*Z*)-isomer therefore provides the advantage of optically controlled activation at the target site. Molecular modelling indicated an avenue to obtain (*Z*)-active LXR agonists from the T0901317 azolog **4** by extension of the unsubstituted phenyl motif (blue ring, Figure 1c). Investigation of the docking poses of three chlorophenyl derivatives of **4** revealed docking scores indicating (*Z*)-preference for the 2-chloro phenyl motif (**7**, Scheme 2). A 3,5-dimethylphenyl motif (**10**, Scheme 2) also showed distinctive docking parameters favouring the (*Z*)-isomer.

Therefore, we prepared the azologs **4**–**14** using Baeyer-Mills coupling between the respective aniline derivatives **15**–**21** and **23**–**24** (Scheme 2). Oxidation of anilines **15**–**21** with oxone resulted in the formation of the corresponding nitrosoarene intermediates, which were used without further purification. Although the oxidation step typically requires 16 h, the electron rich anilines (such as 3,5-dimethylaniline and 2-isopropylaniline) showed fast consumption within 30 min to 5 h, and prolonged stirring caused overoxidation. Reacting these nitrosoarenes with aniline **23** or **24**[23] in acetic acid afforded the desired azobenzenes **4**–**14** in moderate to good yields.

LXR agonism of compounds **4**–**11** was determined in HEK293T cells using Gal4-hybrid reporter gene assays (Figure 2). While the 4-chloro (**5**) and 3-chloro (**6**) regioisomers

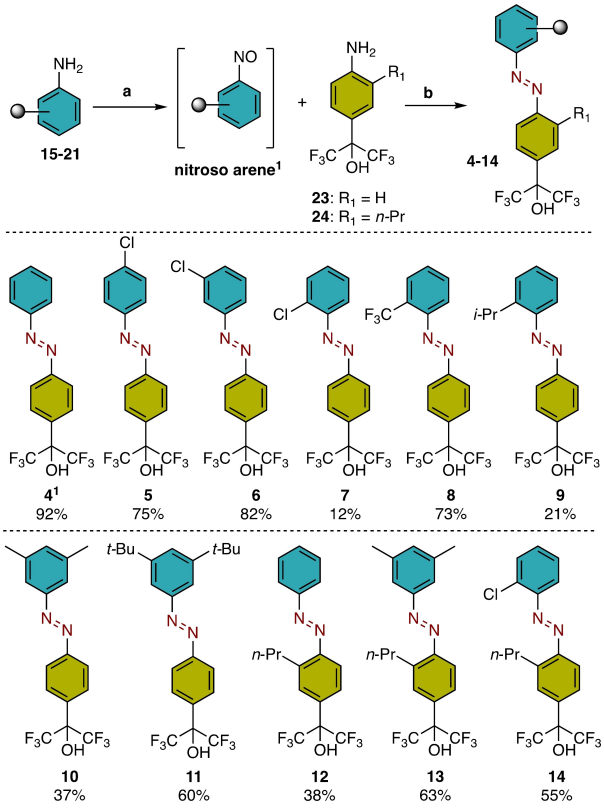

Scheme 2. Synthesis of photoswitchable T0901317 analogues **4**–**14**. Reagents & Conditions: (a) Oxone (6 equiv.), CH_2Cl_2, H_2O, 25 °C, 30 min to 16 h; (b) AcOH (1 mL), 25 °C. [1]**4** was prepared from commercially available nitrosobenzene.

© 2023 The Authors. ChemMedChem published by Wiley-VCH GmbH

18607187, 2023, 11, Downloaded from https://chemistry-europe.onlinelibrary.wiley.com/doi/10.1002/cmdc.202200647, Wiley Online Library on [21/03/2024]. See the Terms and Conditions (https://onlinelibrary.wiley.com/terms-and-conditions) on Wiley Online Library for rules of use; OA articles are governed by the applicable Creative Commons License

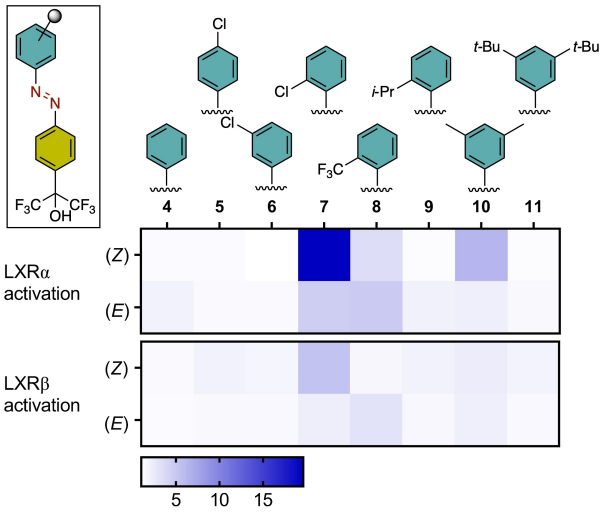

Figure 2. Effect of the substituent modification on the blue arene ring shown by the heat map as the activity of the resulting azobenzenes **4**–**11** towards LXRα and LXRβ activation at the dark (*E*)- and light-activated (*Z*)-states. All compounds were tested at 10 μM in Gal4-hybrid reporter gene assays. A cell-DISCO[21] was used to maintain the light-activated (*Z*)-state. Data are the mean fold activations (vs. 0.1 % DMSO), n ≥ 3.

were not active, in vitro characterization of the 2-chlorophenyl derivative **7** revealed LXR agonism with considerably stronger LXR activation by the light-activated (*Z*)-**7** compared to the (*E*)-**7** isomer as indicated by docking. This result suggested favourable binding of 2-substited azologs of T0901317, which prompted us to study alternative substituents. However, 2-trifluoromethyl (**8**) and 2-isopropyl (**9**) analogues turned out to be less active. Molecular docking had additionally suggested a 3,5-dimethylphenyl motif (**10**) to offer (*Z*)-preferred binding, which was experimentally confirmed albeit with weaker LXR agonism compared to **7**. Steric extension of **10** to the 3,5-di-*tert*-butyl analogue **11** was not tolerated. Thus, the 2-chlorophenyl azolog **7** and the 3,5-dimethylphenyl derivative **10** emerged as the most promising candidates to obtain a photo-activatable LXR agonist. Full dose-response characterization revealed LXR agonism with low micromolar potency and confirmed remarkably higher LXR activation efficacy of the corresponding (*Z*)-isomers (Figure 2 and Table 1).

While the light-activated (*Z*)-**7** and (*Z*)-**10** were more efficient towards LXR activation than the corresponding (*E*)-isomers, this preference was not reflected in EC_{50} values and additional optimization was needed. Further virtual binding mode inspection and comparison with T0901317 indicated that the region occupied by the trifluoroethyl motif of T0901317 could provide an opportunity to reintroduce a substituent to lock the (*Z*)-isomer in a binding mode that would not allow binding of the (*E*)-isomer (Figure 3, Supporting Information Figure 1). Among C_1-C_4 alkyl substituents, docking indicated preference for a propyl chain to occupy the trifluoroethyl binding region. Indeed, the computationally suggested modification **12**, which bears a propyl group (green arene ring, Scheme 2), resulted in a strong preference for the (*Z*)-isomer in terms of activation efficacy, but not an increase

Table 1. Quantified activity of **7** and **10** on LXRα and LXRβ at the dark (*E*)- and light-activated (*Z*)-state. A cell-DISCO[21] was used to maintain the light-activated (*Z*)-state. Max. fold activation refers to fold reporter activity compared to DMSO (0.1 %). Data are the mean ± S.E.M., n ≥ 3.

ID	EC_{50}(LXRα) [max. act.]		EC_{50}(LXRβ) [max. act.]	
	(*E*)-isomer	(*Z*)-isomer	(*E*)-isomer	(*Z*)-isomer
7	13 ± 1 μM [13 ± 2-fold]	13 ± 3 μM [55 ± 9-fold]	14 ± 3 μM [5.9 ± 1.5-fold]	14 ± 2 μM [19 ± 3-fold]
10	17 ± 2 μM [6.2 ± 0.7-fold]	18 ± 1 μM [42 ± 1-fold]	20 ± 2 μM [7.3 ± 1.1-fold]	14 ± 1 μM [10.2 ± 0.8-fold]

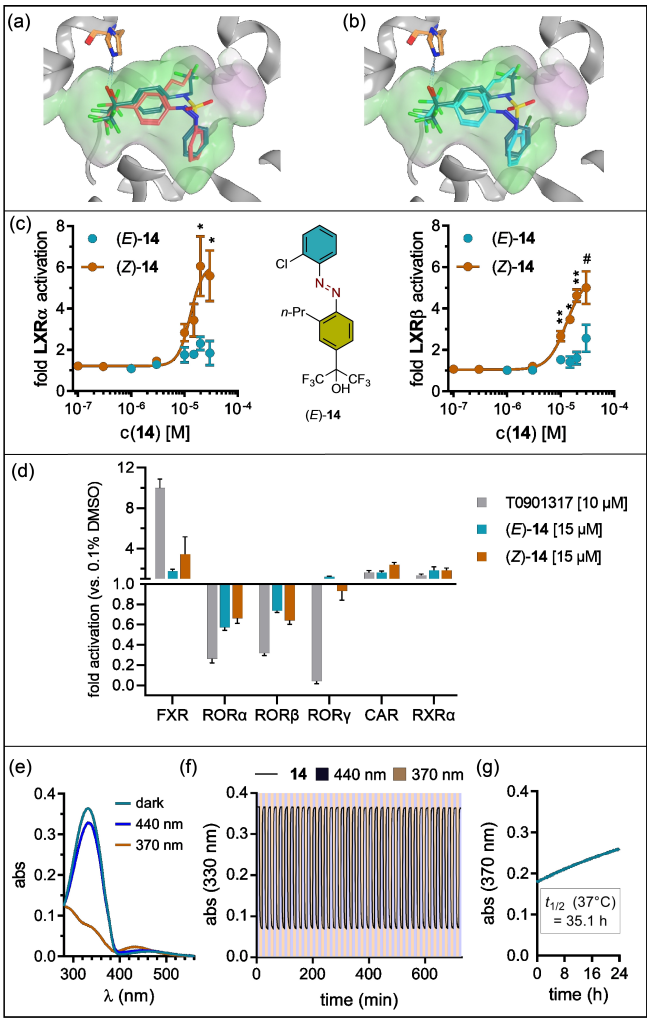

Figure 3. (a,b) Docking of the T0901317 azolog (*Z*)-**12** (a) with propyl substituent and the combined derivative (*Z*)-**14** (b) with propyl and chloro substituent to the LXRβ LBD (pdb ID 1pqc).[22] T0901317: petrol; (*Z*)-**12**: rose-pink; (*Z*)-**14**: cyan. (c) Dose response curves of compound **14** for the activation of LXRα and LXRβ. (*Z*)-**14** was illuminated with λ = 365 nm for 3 min before incubation and maintained in (*Z*)-state with the cell-DISCO[21] system. Fold activation refers to 0.1 % DMSO. Data are the mean ± S.E.M., n ≥ 3. Statistical significance is indicated between (*E*)- and (*Z*)-**14** at the same concentration; # $p < 0.1$, * $p < 0.05$, ** $p < 0.01$ (t-test). (d) Selectivity profiling of (*E*)- and (*Z*)-**14** (15 μM) on known off-targets of the template T0901317 (RORs, FXR, CAR) and on RXRα. T0901317 (10 μM) for comparison. Data are the mean ± S.E.M.; n = 3. (e) UV-vis spectra of **14** (20 μM) in DMSO. (f) Reversible photoswitching of **14** between its (*E*)- and (*Z*)-isomer with alternating illumination at 370 and 440 nm. (g) Thermal relaxation of (*Z*)-**14** (20 μM) at 37 °C in DMSO.

© 2023 The Authors. ChemMedChem published by Wiley-VCH GmbH

18607187, 2023, 11, Downloaded from https://chemistry-europe.onlinelibrary.wiley.com/doi/10.1002/cmdc.202200647, Wiley Online Library on [21/03/2024]. See the Terms and Conditions (https://onlinelibrary.wiley.com/terms-and-conditions) on Wiley Online Library for rules of use; OA articles are governed by the applicable Creative Commons License

in potency (Table 2). Combination of the propyl group with the 3,5-dimethylphenyl moiety of **10** in **13** was not productive but combination with the 2-chlorophenyl motif of **7** generated the light-activatable LXR agonist **14**. Notably, (*Z*)-**14** exhibited LXR agonism with low micromolar potency while no LXR activation was detected for its (*E*)-isomer (Figure 3c and Table 2). Selectivity profiling of (*E*)- and (*Z*)-**14** on RORs, FXR and CAR, which are modulated by the template T0901317, demonstrated reduced off-target activity of **14** (Figure 3d). Additionally, **14** did not activate RXRα, which is the heterodimer partner of LXR. The photophysical properties of **14** were favourable enabling efficient and reversible switching with slow thermal relaxation (Figure 3e–g). Irradiation of 370 nm allowed for switching to the (*Z*)-isomer with a photostationary state (PSS) of 57:43 (*E:Z*), the highest among the active compounds. Compound **14** did not show any fatigue during multiple cycles of photochemical isomerization (370–440 nm) over 10 h (Figure 3f). In the absence of any irradiation, the (*Z*)-isomer requires a half-life of 35.1 h at 37 °C in DMSO (20 μM) to switch back to the (*E*)-form (Figure 3g).

Observation of LXR activity in response to (*E*)-**14** and (*Z*)-**14** over time demonstrated no effect of the inactive (*E*)-isomer while the light-activated (*Z*)-isomer caused continuous cellular LXR activation in a fluorescent protein (mCherry) based reporter gene assay (Figure 4a). With its favourable characteristics and (*Z*)-preferential LXR agonism in firefly and mCherry based reporter gene assays for LXR activation, **14** thus emerged as a valuable early tool to study spatiotemporal control of LXR.

LXR is increasingly gaining attention for its involvement in cancer and its ability to sensitize certain cancer cells for chemotherapeutic treatment. Antiproliferative effects of LXR activation have been hypothesized to involve the alteration of tumour metabolism and signal transduction, inhibition of growth pathways, and activation of apoptotic processes.[9,24] To preliminarily evaluate the potential of light activated LXR agonism in cancer treatment, we tested the ability of **14** to sensitize lung cancer cells (A549) to the kinase inhibitor gefitinib (Figure 4b).[25] Treatment of A549 cells with gefitinib at a low 5 μM concentration was insufficient to cause apoptosis. The LXR agonist **14** (15 μM) exhibited a slight apoptosis inducing activity. However, combination of gefitinib (5 μM) and **14** (15 μM) caused significantly enhanced apoptosis compared to the single treatments. Therein, **14** acted in a light-dependent manner with significantly higher effect of the light-activated form (Figure 4b) indicating that the LXR agonist synergized with gefitinib. This suggests that local LXR activation by light-controlled LXR agonists may have potential as adjuvant cancer treatment by sensitizing cancer cells to other chemotherapeutics. Such strategy may help reducing effective doses of anticancer drugs thus lowering systemic side effects.

Table 2. Activity of the photoswitchable LXR agonists **12** and **14** in (*E*)- and (*Z*)-state on LXRα and LXRβ in Gal4-hybrid reporter gene assays. A cell-DISCO[21] was used to maintain the light-activated (*Z*)-state. Max. fold activation refers to fold reporter activity compared to DMSO (0.1 %). Data are the mean ± S.E.M., n ≥ 3. Inactive – no statistically significant LXR activation at the indicated concentration.

ID	EC_{50}(LXRα) [max. act.]		EC_{50}(LXRβ) [max act.]	
	(*E*)-isomer	(*Z*)-isomer	(*E*)-isomer	(*Z*)-isomer
12	17 ± 1 μM [5.2 ± 0.4-fold]	11 ± 1 μM [34 ± 2-fold]	17 ± 1 μM [30 ± 2-fold]	13.0 ± 0.4 μM [35 ± 1-fold]
14	inactive (30 μM)	13 ± 3 μM [6.1 ± 1.3-fold]	inactive (30 μM)	13 ± 3 μM [5.5 ± 1.1-fold]

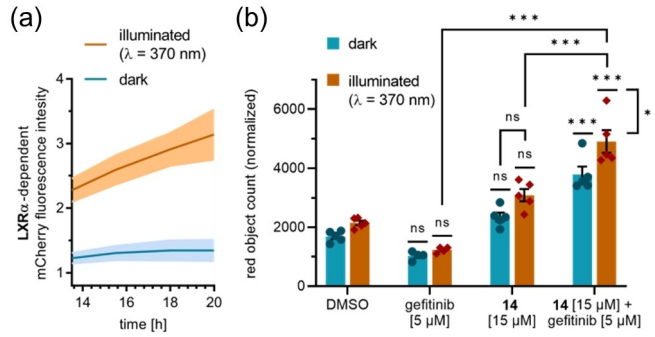

Figure 4. In vitro characterization of **14**. (a) Light-activated (*Z*)-**14** (10 μM, orange) continuously induced LXRα dependent mCherry expression in living cells. (*E*)-**14** (10 μM, blue) had no effect. A cell-DISCO[21] was used to maintain the light-activated (*Z*)-state. Lines are the mean, shadows represent S.E.M.; n = 3. (b) **14** sensitized A549 lung cancer cells for gefitinib induced apoptosis in a light-dependent fashion. Apoptosis was determined by propidium iodide staining. A cell-DISCO[21] was used to maintain the light-activated (*Z*)-state. Data are the mean ± S.E.M., n ≥ 4. Statistical significance is shown compared to DMSO (0.1 %) or as indicated; ns (not significant) $p \geq 0.05$, * $p < 0.05$, *** $p < 0.001$ (ANOVA with Bonferroni correction).

Conclusion

LXR activation as therapeutic strategy in metabolic diseases has encountered failures due to limiting adverse effects on hepatic lipid metabolism. Although recent findings highlight LXR as potential target in cancer treatment, systemic adverse effects of LXR agonists remain a challenge. By enabling light-induced local activation, photopharmacology may provide a solution to this problem. Based on the long-known T0901317 scaffold, we have developed the LXR agonist **14** that activates LXR only in its light-induced (*Z*)-state thereby enabling spatiotemporal control of LXR activity. Despite its moderate potency, **14** sensitized human lung cancer cells against gefitinib treatment in a light-dependent fashion and validates the concept of optical control of LXR. It may serve as an early chemical tool and as a valuable lead to develop light activated LXR agonists with improved potency and activation efficacy.

Experimental Section

Chemistry

Materials and Methods: All reagents and solvents were purchased from commercial sources (Sigma-Aldrich, TCI Europe N.V., Strem Chemicals, Santa Cruz Biotechnology Inc., Oakwood chemicals) and were used without further purification unless otherwise stated. Reactions were monitored by thin layer chromatography

© 2023 The Authors. ChemMedChem published by Wiley-VCH GmbH

18607187, 2023, 11, Downloaded from https://chemistry-europe.onlinelibrary.wiley.com/doi/10.1002/cmdc.202200647, Wiley Online Library on [21/03/2024]. See the Terms and Conditions (https://onlinelibrary.wiley.com/terms-and-conditions) on Wiley Online Library for rules of use; OA articles are governed by the applicable Creative Commons License

(TLC) on pre-coated, Silica gel F254 TLC plates from Merck KGaA using UV irradiation at $\lambda = 254$ nm as the visualizing agent or appropriate staining solution. Purification by column chromatography was performed using either manual air pressure or a Teledyne Isco Combiflash Rf+ UV purification system on Geduran© si60 silica gel (40–63 μm) from Merck KGaA.

Nuclear Magnetic Resonance (NMR) Spectroscopy: NMR solvents were acquired from Cambridge Isotope Laboratories. NMR spectra were measured on a BRUKER Avance III HD 400. Multiplicities in the following experimental procedures are abbreviated as follows: s = singlet, d = doublet, t = triplet, q = quartet, hept = heptet, m = multiplet, br = broad and combination thereof. ^{1}H chemical shifts are expressed in parts per million (ppm, δ scale) and are referenced to the residual protium in the NMR solvent ($CDCl_3$: δ = 7.26). ^{13}C chemical shifts are expressed in ppm (δ scale) and are referenced to the carbon resonance of the NMR solvent ($CDCl_3$: δ = 77.16). $CDCl_3$ was neutralized by filtering through K_2CO_3 plug and storing over 4 Å MS.

Photophysical Characterization: UV-Vis spectra were recorded using a Varian Cary 50 Bio UV-Visible Spectrophotometer. Photoswitching was achieved using 365 nm or 460 nm LED light sources. The light source was pointed directly onto the top of the sample cuvette with sample concentrations of 20 μM in DMSO. All experiments were carried out at 37 °C. Absorption spectra were recorded at different irradiation wavelengths (320–550 nm) starting from no irradiation. For photostability experiments, the maximum absorption wavelength (λ_{max}) was monitored with a repeated irradiation program set with 370 nm (5 min) and 440 nm (5 min) and was cycled for minimum 1 h. For thermal relaxation, each sample was first irradiated with 370 nm for 10–15 min to ensure complete switching into the (*Z*)-form, and then the samples were allowed to switch back to the (*E*)-isomer. Photostationary states (PSS) of the most relevant compounds **7** (*E*:*Z* = 76:24), **10** (*E*:*Z* = 60:40), **12** (*E*:*Z* = 72:28), and **14** (*E*:*Z* = 57:43) were determined by irradiating a DMSO-d_6 solution (1 mM) with 370 nm LED plate (low power) for 30 min. The NMR tubes were kept at dark and ^{1}H NMR spectra were collected in a 400 MHz instrument.

General procedure for the preparation of azobenzene analogues 5–14: The respective substituted aniline **15**–**21** (2.0 equiv. with respect to starting material **23** or **24**) was dissolved in CH_2Cl_2 (0.06 M), treated with a solution of Oxone® (6.0 equiv.) in H_2O (0.35 M), and the resulting biphasic mixture was stirred vigorously at room temperature until the complete consumption of aniline. The two phases were separated, and the organic phase was washed with 1 M HCl, saturated $NaHCO_3$ solution, and H_2O. The organic phase was dried over Na_2SO_4 and filtered to isolate the nitroso intermediate. A solution of 2-(4-aminophenyl)-1,1,1,3,3,3-hexafluoropropan-2-ol derivative **23** (1.0 equiv.) or 2-(4-amino-3-propylphenyl)-1,1,1,3,3,3-hexafluoropropan-2-ol (**24**, 1.0 equiv.) in CH_2Cl_2 (0.2 M) was added, followed by AcOH (0.1 M). The CH_2Cl_2 was removed under reduced pressure, and the resulting solution was stirred at room temperature overnight. AcOH was removed under reduced pressure and the crude oil was purified by flash column chromatography (SiO_2, gradient: 0–50% *n*-hexane/EtOAc) to yield the desired azobenzene products **4**–**14**.

(E)-1,1,1,3,3,3-hexafluoro-2-(4-(phenyldiazenyl)phenyl)propan-2-ol (4)

Prepared by stirring commercially available nitrosobenzene (35 mg, 0.327 mmol, 1.5 equiv.) and 2-(4-aminophenyl)-1,1,1,3,3,3-hexafluoropropan-2-ol (**23**, 58 mg, 0.224 mmol, 1.0 equiv.) in glacial acetic acid (1.5 mL) for 12 h. Acetic acid was removed in vacuo and the resulting red residue was azeotroped with toluene (2 × 5 mL). The residue was then purified by flash chromatography. Elution of 30% EtOAc in hexane afforded the desired azobenzene **4** as orange solid (72 mg, 0.207 mmol, 92% yield). $R_f = 0.50$ (20% EtOAc in hexane). ^{1}H NMR (400 MHz, $CDCl_3$): δ = 8.01–7.93 (m, 4 H), 7.89 (m, 2 H), 7.57–7.549 (m, 3 H), 3.47 (s, 1 H). ^{13}C NMR (101 MHz, $CDCl_3$): δ = 153.7, 152.7, 131.7, 131.4, 129.3, 127.7, 127.7, 124.1, 123.2, 122.9, 121.3. HRMS (ESI TOF): *m/z* calcd. for $C_{15}H_{11}F_6N_2O^+$ ($[M+H]^+$) 349.0776; found 349.0772 ($[M+H]^+$).

((E)-2-(4-((4-chlorophenyl)diazenyl)phenyl)-1,1,1,3,3,3-hexafluoropropan-2-ol (5)

4-Chloroaniline (**16**, 29.5 mg, 0.232 mmol, 2.0 equiv.) was subjected to the conditions described in the general procedure to yield **5** (33.3 mg, 0.087 mmol, 75%) as an orange oil. $R_f = 0.52$ (20% EtOAc in hexane). ^{1}H NMR (400 MHz, $CDCl_3$): δ = 7.99–7.96 (m, 2 H), 7.90–7.88 (m, 4 H), 7.53–7.49 (m, 2 H). ^{13}C NMR (101 MHz, $CDCl_3$): δ = 153.5, 151.0, 137.8, 131.7, 129.6, 129.2, 127.7, 124.5, 124.1, 123.0. (Major (*E*)-isomer is reported; small quantity (12%) of minor (*Z*)-isomer was observed). HRMS (ESI TOF): *m/z* calcd. for $C_{15}H_{10}ClF_6N_2O^+$ ($[M+H]^+$) 383.0386; found 383.0380 ($[M+H]^+$).

(E)-2-(4-((3-chlorophenyl)diazenyl)phenyl)-1,1,1,3,3,3-hexafluoropropan-2-ol (6)

3-Chloroaniline (**17**, 29.5 mg, 0.232 mmol, 2.0 equiv.) was subjected to the conditions described in the general procedure to yield **6** (36.4 mg, 0.095 mmol, 82%) as an orange oil. $R_f = 0.45$ (20% EtOAc in hexane). ^{1}H NMR (400 MHz, $CDCl_3$): δ = 8.00–7.98 (m, 2 H), 7.92–7.91 (m, 2 H), 7.89 (br s, 1 H), 7.87–7.84 (m, 1 H), 7.49–7.47 (m, 2 H), 3.50 (s, 1 H). ^{13}C NMR (101 MHz, $CDCl_3$): δ = 153.4, 153.3, 135.4, 132.0, 131.4, 130.4, 127.8, 124.1, 123.1, 122.8, 122.1, 121.2, 121.2. HRMS (ESI-TOF): *m/z* calcd. for $C_{15}H_{10}ClF_6N_2O^+$ ($[M+H]^+$) 383.0386; found 383.0381 ($[M+H]^+$).

(E)-2-(4-((2-chlorophenyl)diazenyl)phenyl)-1,1,1,3,3,3-hexafluoropropan-2-ol (7)

2-Chloroaniline (**18**, 29.5 mg, 0.232 mmol, 2.0 equiv.) was subjected to the conditions described in the general procedure to yield **7** (5.4 mg, 0.014 mmol, 12%) as an orange oil. $R_f = 0.42$ (20% EtOAc in hexane). ^{1}H NMR (400 MHz, $CDCl_3$): δ = 8.04 (d, J = 8.9 Hz, 2 H), 7.90 (d, J = 9.0 Hz, 2 H), 7.71 (dd, J = 8.0, 1.8 Hz, 1 H), 7.58 (dd, J = 8.0, 1.4 Hz, 1 H), 7.43 (td, J = 7.7, 1.7 Hz, 1 H), 7.39–7.33 (m, 1 H), 3.52 (s, 1 H). ^{13}C NMR (101 MHz, $CDCl_3$): δ = 153.7, 148.8, 136.0, 132.4, 132.0, 131.0, 127.8, 127.5, 124.1, 123.4, 121.2, 117.7. HRMS (ESI-TOF): *m/z* calcd. for $C_{15}H_{10}ClF_6N_2O^+$ ($[M+H]^+$) 383.0386; found 383.0381 ($[M+H]^+$).

(E)-1,1,1,3,3,3-hexafluoro-2-(4-((2-(trifluoromethyl)phenyl)diazenyl)phenyl)propan-2-ol (8)

2-(Trifluoromethyl)aniline (**19**, 512 mg, 3.18 mmol, 2.0 equiv.) was dissolved in CH_2Cl_2 (30 mL) and a solution of Oxone® (5.86 g, 9.53 mmol, 6.0 equiv.) in H_2O (20 mL) was added. The biphasic mixture was stirred for 16 h. Light green suspension was obtained. Two layers were separated. Organic layer was washed with 1 M HCl (30 mL), sat. $NaHCO_3$ (40 mL), and H_2O (40 mL). Dried over Na_2SO_4 and concentrated. To the vibrant green oil in CH_2Cl_2 (8 mL) was added 2-(4-aminophenyl)-1,1,1,3,3,3-hexafluoropropan-2-ol (**23**, 412 mg, 1.59 mmol, 1.0 equiv.) as solid. AcOH (6 mL) was added, CH_2Cl_2 was removed under vacuum and the mixture was stirred at room temperature for 20 h. AcOH were removed under

© 2023 The Authors. ChemMedChem published by Wiley-VCH GmbH

18607187, 2023, 11, Downloaded from https://chemistry-europe.onlinelibrary.wiley.com/doi/10.1002/cmdc.202200647, Wiley Online Library on [21/03/2024]. See the Terms and Conditions (https://onlinelibrary.wiley.com/terms-and-conditions) on Wiley Online Library for rules of use; OA articles are governed by the applicable Creative Commons License

vacuum. EtOAc (30 mL) was added followed by sat. $NaHCO_3$ (60 mL) (vigorous bubbling). Stirred for 10 min. Layers were separated. Organic layer was washed with H_2O (40 mL), dried over Na_2SO_4. Solvents were removed and the crude orange residue was purified by flash chromatography using 40% EtOAc in hexane to isolate bright orange crystalline solid as the desired azobenzene **8** (484 mg, 1.16 mmol, 73% yield). $R_f = 0.42$ (20% EtOAc in hexane). ^{1}H NMR (400 MHz, $CDCl_3$): $\delta = 8.05$ (d, $J = 8.9$ Hz, 2 H), 7.92 (d, $J =$ 8.5 Hz, 2 H), 7.87–7.83 (m, 2 H), 7.69–7.65 (m, 1 H), 7.62–7.58 (m, 1 H), 3.43 (s, 1 H). ^{13}C NMR (101 MHz, $CDCl_3$): $\delta = 153.5$, 149.4, 132.8, 132.3, 131.1, 129.1 (q, $J_{C-F} = 31.2$ Hz, CF_3), 127.8, 126.8 (q, $J_{C-F} = 5.4$ Hz, CCF_3), 125.4, 124.1, 123.6, 122.7, 116.3. HRMS (ESI-TOF): *m/z* calcd. for $C_{16}H_8F_9N_2O^-$ ($[M-H]^-$) 415.0493; found 415.0502 ($[M-H]^-$).

(E)-1,1,1,3,3,3-hexafluoro-2-(4-((2-isopropylphenyl)diazenyl)phenyl)propan-2-ol (9)

2-isopropylaniline (**20**, 52.2 mg, 0.386 mmol, 2.0 equiv.) and 2-(4-aminophenyl)-1,1,1,3,3,3-hexafluoropropan-2-ol (**23**, 50 mg, 0.193 mmol, 1.0 equiv.) was subjected to the conditions of the general procedure to yield **9** (25 mg, 0.064 mmol, 33%) as an orange oil. ***(Note**: the oxidation step using Oxone® showed complete consumption of 2-isopropyl aniline within 5 h).* $R_f = 0.56$ (20% EtOAc in hexane). ^{1}H NMR (400 MHz, $CDCl_3$): $\delta = 8.01$–7.97 (m, 2 H), 7.90 (d, $J = 8.5$ Hz, 2 H), 7.63 (d, $J = 8.0$ Hz, 1 H), 7.49–7.47 (m, 2 H), 7.30–7.27 (m, 1 H), 4.11 (hept, $J = 7.0$ Hz, 1 H), 1.36 (d, $J = 7.0$ Hz, 6 H). ^{13}C NMR (101 MHz, $CDCl_3$): $\delta = 153.8$, 149.5, 148.5, 131.9, 131.1, 127.6, 126.5, 126.3, 124.0, 122.9, 120.7, 115.2, 27.8, 23.9. HRMS (ESI-TOF): *m/z* calcd. for $C_{18}H_{17}F_6N_2O^+$ ($[M+H]^+$) 391.1245; found 391.1240 ($[M+H]^+$).

(E)-1,1,1,3,3,3-hexafluoro-2-(4-((3,5-di-methylphenyl)diazenyl)phenyl)-propan-2-ol (10)

3,5-dimethylaniline (**21**, 28.1 mg, 0.232 mmol, 2.0 equiv.) was subjected to the conditions described in the general procedure to yield **10** (16.2 mg, 0.043 mmol, 37%) as an orange oil. $R_f = 0.52$ (20% EtOAc in hexane). ***(Note**: the oxidation step with Oxone® required only 30 min for complete consumption of the aniline. Stirring for longer time causes overoxidation to nitro).* ^{1}H NMR (400 MHz, $CDCl_3$): $\delta = 7.98$–7.95 (m, 2 H), 7.88 (d, $J = 8.5$ Hz, 2 H), 7.56 (br s, 2 H), 7.16 (s, 1 H), 3.46 (s, 1 H, OH), 2.43 (s, 6 H, CH_3). ^{13}C NMR (101 MHz, $CDCl_3$): $\delta = 153.8$, 152.9, 139.0, 133.1, 131.2, 127.7, 124.1, 122.8, 121.3, 121.0, 21.4. HRMS (ESI-TOF): *m/z* calcd. for $C_{17}H_{15}F_6N_2O^+$ ($[M+H]^+$) 377.1089; found 377.1085 ($[M+H]^+$).

(E)-2-(4-((3,5-di-tert-butylphenyl)diazenyl)phenyl)-1,1,1,3,3,3-hexafluoropropan-2-ol (11)

3,5-di-tert-butylaniline (**22**, 47.5 mg, 0.232 mmol, 2.0 equiv.) was subjected to the conditions described in the general procedure to yield **11** (32.0 mg, 0.070 mmol, 60%) as an orange oil. $R_f = 0.54$ (20% EtOAc in hexane). ^{1}H NMR (400 MHz, $CDCl_3$): $\delta = 7.97$ (d, $J =$ 8.5 Hz, 2 H), 7.87 (d, $J = 8.4$ Hz, 2 H), 7.80 (br s, 2 H), 7.60 (br s, 1 H), 3.48 (s, 1H, OH), 1.41 (s, 18H, t-Bu). ^{13}C NMR (101 MHz, $CDCl_3$): $\delta =$ 154.0, 152.7, 152.1, 131.0, 127.6, 126.1, 124.1, 122.8, 121,3, 117.7, 35.3, 31.6. HRMS (ESI-TOF): *m/z* calcd. for $C_{23}H_{27}F_6N_2O^+$ ($[M+H]^+$) 461.2028; found 461.2022 ($[M+H]^+$).

(E)-1,1,1,3,3,3-hexafluoro-2-(4-(phenyldiazenyl)-3-propylphenyl)propan-2-ol (12)

Aniline (**15**, 150 mg, 1.61 mmol, 2.0 equiv.) was dissolved in CH_2Cl_2 (15 mL), treated with a solution of Oxone® (2.97 g, 4.83 mmol, 6.0 equiv.) in H_2O (10 mL), and the resulting biphasic mixture was stirred rapidly at room temperature 16 h. A red-orange mixture formed. The two phases were separated, and the organic phase was washed with 1 M HCl (3×20 mL), sat. $NaHCO_3$ solution (25 mL), and H_2O (25 mL). The organic phase was dried over Na_2SO_4 and filtered. Concentrated to 2 mL and 2-(4-amino-3-propylphenyl)-1,1,1,3,3,3-hexafluoropropan-2-ol (**24**, 243 mg, 0.805 mmol, 1.0 equiv.) was added as solid, followed by AcOH (2 mL). CH_2Cl_2 was removed under reduced pressure, and the resulting solution was stirred at room temperature for 14 h. AcOH was removed under reduced pressure to obtain a red-orange residue. It was dissolved in Et_2O (0.5 mL) and hexane (5 mL) was added and upon cooling overnight crystals of unreacted **24** were isolated. The mother liquor was dried under vacuum and purified by flash column chromatography using 30–50% gradient of EtOAc in hexanes. The desired azobenzene product **12** was isolated as an orange oil (121 mg, 0.310 mmol, 38% yield). $R_f = 0.51$ (20% EtOAc in hexane). ^{1}H NMR (400 MHz, $CDCl_3$): $\delta = 7.95$–7.93 (m, 2 H), 7.71–7.67 (m, 2 H), 7.64–7.62 (m, 1 H), 7.56–7.49 (m, 3 H), 3.43 (s, 1H), 3.15 (t, $J = 7.5$ Hz, 2 H), 1.77–1.67 (m, 2 H), 0.97 (t, $J = 7.4$ Hz, 3 H). ^{13}C NMR (101 MHz, $CDCl_3$): $\delta = 153.0$, 151.6, 142.5, 131.5, 131.2, 129.3, 129.0, 124.9, 124.2, 123.3, 121.3, 115.9, 33.8, 25.2, 14.0. HRMS (ESI-TOF): *m/z* calcd. for $C_{18}H_{16}F_6NaN_2O^+$ ($[M+Na]^+$) 413.1065; found 413.1050 ($[M+Na]^+$).

(E)-1,1,1,3,3,3-hexafluoro-2-(4-((3,5-di-methylphenyl)diazenyl)-3-propylphenyl)- propan-2-ol (13)

3,5-Dimethylaniline (**21**, 40.2 mg, 0.332 mmol, 2.0 equiv.) was dissolved in CH_2Cl_2 (15 mL) and Oxone® (612 mg, 0.996 mmol, 6.0 equiv.) in H_2O (15 mL) was added to it. Stirred vigorously over 10 min to obtain a brown-red biphasic mixture. TLC showed complete consumption of the aniline and a new spot. ***(Note**: the oxidation step with Oxone® required only 30 min for complete consumption of the aniline. Stirring for longer time causes over-oxidation to nitro).* Two layers were separated. Aqueous layer was extracted with CH_2Cl_2 (2×20 mL). Organic layer was washed with 1 M HCl (3×15 mL), sat. $NaHCO_3$ (2×15 mL) and H_2O (25 mL). Organic layer was dried over Na_2SO_4 and filtered. To the CH_2Cl_2 solution, was added 2-(4-amino-3-propylphenyl)-1,1,1,3,3,3-hexafluoropropan-2-ol (**24**, 50 mg, 0.166 mmol, 1.0 equiv.) as solid and AcOH (3 mL) was added. CH_2Cl_2 was removed under reduced pressure and the resulting red solution was stirred at room temperature for 14 h. AcOH was removed under vacuum. The dark red residue was purified by flash chromatography using 20% EtOAc in hexane to isolate the desired azobenzene **13** as an orange glue (44 mg, 0.110 mmol, 63% yield). $R_f = 0.51$ (10% EtOAc in hexane). ^{1}H NMR (400 MHz, $CDCl_3$): $\delta = 7.70$ (s, 1 H), 7.63–7.62 (m, 2 H), 7.54 (br s, 2 H), 7.15 (br s, 1 H), 3.44 (s, 1 H), 3.16–3.12 (m, 2 H), 2.44 (s, 6 H), 1.76–1.67 (m, 2 H), 0.97 (t, $J = 7.4$ Hz, 3 H). ^{13}C NMR (101 MHz, $CDCl_3$): $\delta = 153.3$, 151.8, 142.2, 139.0, 133.2, 131.0, 128.9, 124.9, 123.2, 121.1, 120.2, 115.9, 33.5, 25.2, 21.5, 14.0. HRMS (ESI-TOF): *m/z* calcd. for $C_{20}H_{21}F_6N_2O^+$ ($[M+H]^+$) 419.1553; found 419.1543 ($[M+H]^+$).

(E)-2-(4-((2-chlorophenyl)diazenyl)-3-propylphenyl)-1,1,1,3,3,3-hexafluoropropan-2-ol (14)

2-Chlorolaniline (**18**, 42.3 mg, 0.332 mmol, 2.0 equiv.) was dissolved in CH_2Cl_2 (15 mL) and Oxone® (612 mg, 0.996 mmol, 6.0 equiv.) in H_2O (15 mL) was added to it. Stirred vigorously at

© 2023 The Authors. ChemMedChem published by Wiley-VCH GmbH

18607187, 2023, 11, Downloaded from https://chemistry-europe.onlinelibrary.wiley.com/doi/10.1002/cmdc.202200647, Wiley Online Library on [21/03/2024]. See the Terms and Conditions (https://onlinelibrary.wiley.com/terms-and-conditions) on Wiley Online Library for rules of use; OA articles are governed by the applicable Creative Commons License

25 °C for 16 h to obtain a green biphasic mixture. TLC showed complete consumption of the aniline with a new spot. Two layers were separated. Aqueous layer was extracted with CH_2Cl_2 (2× 20 mL). Organic layer was washed with 1 M HCl (3×15 mL), sat. $NaHCO_3$ (2×15 mL) and H_2O (25 mL). Organic layer was dried over Na_2SO_4 and filtered. To the CH_2Cl_2 solution, was added 2-(4-amino-3-propylphenyl)-1,1,1,3,3,3-hexafluoropropan-2-ol (**24**, 50 mg, 0.166 mmol, 1.0 equiv.) as solid and AcOH (3 mL) was added. CH_2Cl_2 was removed under reduced pressure and the AcOH solution was stirred for 14 h. AcOH was removed under vacuum and the dark red residue was purified by flash chromatography using 20% EtOAc in hexane to isolate the desired azobenzene **14** as an orange glue (39 mg, 0.092 mmol, 55% yield). $R_f = 0.46$ (10% EtOAc in hexane). ^{1}H NMR (400 MHz, $CDCl_3$): δ = 7.76 (d, J = 8.7 Hz, 1 H), 7.71 (br s, 1 H), 7.68–7.63 (m, 2 H), 7.58 (dd, J = 7.9, 1.5 Hz, 1 H), 7.47–7.35 (m, 3 H), 3.45 (s, 1 H), 3.17 (t, J = 7.5 Hz, 2 H), 1.77–1.68 (m, 2 H), 0.98 (t, J = 7.3 Hz, 3 H). ^{13}C NMR (101 MHz, $CDCl_3$): δ = 151.6, 149.0, 143.0, 136.0, 132.2, 131.8, 131.2, 131.0, 129.1, 127.5, 125.0, 123.1, 121.3, 117.8, 116.5, 33.4, 25.3, 14.0. HRMS (ESI-TOF): *m/z* calcd. for $C_{18}H_{16}ClF_6N_2O^+$ ($[M+H]^+$) 425.0855; found 425.0954 ($[M+H]^+$).

2-(4-amino-3-propylphenyl)-1,1,1,3,3,3-hexafluoropropan-2-ol (24)

Prepared following a reported procedure.[23] Compound **24** was isolated as white powder and the spectral data matched the reported values.

Computational Methods

General: Calculations were performed in Molecular Operating Environment (MOE, version 2022.02, Chemical Computing Group ULC, Montreal, QC, Canada) using default settings for each tool/function unless stated otherwise. Amber10:EHT was used as the default forcefield for all calculations.

Molecular Docking: Docking was performed using the X-ray structure of the LXRβ LBD complexed with T0901317 (**3**, pdb ID 1pqc).[22] Protonation state of the complex was adjusted using the MOE QuickPrep tool. The compounds were prepared using the Energy minimize tool with preserved existing chirality and MOE Wash tool: protonation state dominant at pH 7.0. Docking was performed using the following settings in the MOE Dock tool: receptor: receptor + solvent; site: ligand atoms; placement: Pharmacophore; score: London dG; poses: 100; refinement: induced fit; refinement score: GBVI/WSA dG; poses: 10. As a pharmacophore query, the hydroxyl group of the crystallized ligand was set as an H-bond donor & acceptor feature with a 1.0 radius. Redocking of the crystallized ligand T0901317 (**3**) in LXRβ (pdb ID 1pqc)[22] resulted in a docking score of −10.01 (range −10.01 – −9.16, median −9.64) and an RMSD value of 0.455 (range 0.455–3.457, median 2.458). The RMSD values between the docked poses and the crystallized ligand were calculated with the mol rmsd SVL script in MOE.

In Vitro Pharmacological Characterization

Hybrid Reporter Gene Assays

Plasmids: The Gal4-fusion receptor plasmids pFA-CMV-hLXRα-LBD, pFA-CMV-hLXRβ-LBD, pFA-CMV-hFXR-LBD, pFA-CMV-hRORα-LBD, pFA-CMV-hRORβ-LBD, pFA-CMV-hRORγ-LBD, pFA-CMV-hCAR-LBD, and pFA-CMV-hRXRα-LBD coding for the hinge region and the ligand binding domain of the canonical isoform of the respective nuclear receptor have been reported previously.[26–29] pFR-Luc (Stratagene, La Jolla, CA) was used as the reporter plasmid and pRL-SV40 (Promega, Madison, WI) for normalization of transfection efficiency and cell growth.

Procedure: HEK293T cells were cultured in Dulbecco's modified Eagle's medium (DMEM), high glucose with 10% fetal calf serum (FCS), sodium pyruvate (1 mM), penicillin (100 U/mL), and streptomycin (100 μg/mL) at 37 °C and 5% CO_2. Twenty-four hours before transfection, the cells were seeded in transparent 96-well plates (3×10^4 cells/well). Before transfection, the medium was changed to Opti-MEM without supplements. Transient transfection was carried out using Lipofectamine LTX reagent (Invitrogen, Carlsbad, CA) according to the manufacturer's protocol with pFR-Luc (Stratagene), pRL-SV40 (Promega), and one Gal4-LXR hybrid receptor plasmid. Five hours after transfection, the medium was changed to Opti-MEM supplemented with penicillin (100 U/mL) and streptomycin (100 μg/mL) and additionally containing 0.1% dimethyl sulfoxide (DMSO) and the respective test compound or 0.1% DMSO alone as the untreated control. Each sample was tested in duplicate, and each experiment was repeated independently at least three times. After incubation overnight (14–16 h), the cells were assayed for luciferase activity using the Dual-Glo Luciferase Assay System (Promega) according to the manufacturer's protocol. Luminescence was measured with a Tecan Spark 10 M luminometer (Tecan Group Ltd., Männedorf, Switzerland). Normalization of transfection efficiency and cell growth was done by dividing the firefly luciferase data by Renilla luciferase data and multiplying the value by 1000, resulting in relative light units (RLUs). Fold activation was obtained by dividing the mean RLU of the test compound by the mean RLU of the untreated control. Characterization of the respective (*Z*)-counterparts was performed in the same way with preirradiated compounds (irradiation for 3 min at λ = 365 nm before incubation). To maintain the compound in the (*Z*)-adapted state, the cell-DISCO[21] system was used during incubation with 75 ms light pulses (λ = 370 nm) every 15 s. For dose-response curve fitting and calculation of EC_{50} values, the equation "[Agonist] vs. response-variable slope (four parameters)" was performed with mean fold activations ± SD using GraphPad Prism (version 7.00, GraphPad Software, La Jolla, CA). The hybrid assays were validated with the reference agonist T0901317 (**3**, LXRα: EC_{50} 0.22 ± 0.13 μM (28 ± 6 max. fold act.); LXRβ: EC_{50} 0.21 ± 0.05 μM (20 ± 2 max. fold act.)) which yielded EC_{50} values in agreement with the literature.[30] Selectivity profiling was performed equally using corresponding hybrid receptor plasmids and reference modulators on FXR (pFA-CMV-hFXR-LBD, 1 μM GW4064), RORα (pFA-CMV-hRORα-LBD, 1 μM SR1001), RORβ (pFA-CMV-hRORβ-LBD, 1 μM SR1001), RORγ (pFA-CMV-hRORγ-LBD, 1 μM SR1001), CAR (pFA-CMV-hCAR-LBD, 1 μM CITCO), and RXRα (pFA-CMV-hRXRα-LBD, 1 μM bexarotene).

Fluorescence Reporter Gene Assay

Plasmids: The Gal4-responsive fluorescence reporter mCherry was expressed from plasmid pUAS-mCherry-NLS (Addgene, entry 87695, Watertown, MA).[31] The Gal4-fusion receptor plasmid pFA-CMV-hLXRα-LBD coding for the hinge region and the ligand binding domain of the canonical isoform of the nuclear receptor has been reported previously.[26]

Procedure: HEK293T cells were cultured in DMEM, high glucose with 10% FCS, sodium pyruvate (1 mM), penicillin (100 U/mL), and streptomycin (100 μg/mL) at 37 °C and 5% CO_2. Twenty-four hours before transfection, the cells were seeded in black cell culture 96-well microplates with optical flat bottom (3×10^4 cells/well; Nalge Nunc International, Rochester, NY). Before transfection, the medium was changed to Opti-MEM without supplements. Tran-

© 2023 The Authors. ChemMedChem published by Wiley-VCH GmbH

18607187, 2023, 11, Downloaded from https://chemistry-europe.onlinelibrary.wiley.com/doi/10.1002/cmdc.202200647, Wiley Online Library on [21/03/2024]. See the Terms and Conditions (https://onlinelibrary.wiley.com/terms-and-conditions) on Wiley Online Library for rules of use; OA articles are governed by the applicable Creative Commons License

sient transfection was carried out using Lipofectamine LTX reagent (Invitrogen) according to the manufacturer's protocol with pUASmCherry-NLS (Addgene, entry 87695) and the Gal4-fusion LXRα plasmid. Five hours after transfection, the medium was changed to Opti-MEM supplemented with penicillin (100 U/mL) and streptomycin (100 μg/mL) and additionally containing 0.1% DMSO and the respective test compound or 0.1% DMSO alone as the untreated control. Each sample was tested in duplicate, and each experiment was repeated independently three times. After incubation for 14 h, the living cells were assayed for fluorescence reporter intensity every second hour until 20 h. The fluorescence intensity (FI) was measured after excitation at 585/10 nm with the emission wavelength of 610/10 nm in bottom reading mode with a Tecan Spark Cyto (Tecan Group Ltd.). Fold FI was obtained by dividing the mean FI of the test compound by the mean FI of the untreated control. Hybrid fluorescence assay performance was monitored with the reference agonist T0901317 (**3**) at a concentration of 1 μM. Characterization of the respective (*Z*)-counterpart was performed in the same way with preirradiated compound (irradiation for 3 min at $\lambda = 365$ nm before incubation). To maintain the compound in the (*Z*)-adapted state, the cell-DISCO[21] system was used during incubation with 75 ms light pulses ($\lambda = 370$ nm) every 15 s.

Apoptosis staining

A549 cells were cultured in DMEM, high glucose with 10% FCS, sodium pyruvate (1 mM), penicillin (100 U/mL), and streptomycin (100 μg/mL) at 37 °C and 5% CO_2. The cells were seeded in transparent 96-well plates (5×10^3 cells/well). After 24 h, the medium was refreshed, now additionally containing 0.1% DMSO and the respective test compound (*E*)-**14** or (*Z*)-**14** (each at 15 μM) alone, or the apoptosis inducer gefitinib (5 μM) alone, or a combination of both, or 0.1% DMSO alone as untreated control. Characterization of (*Z*)-**14** was performed with preirradiated compound (irradiation for 3 min at $\lambda = 365$ nm before incubation). To maintain the compound in the (*Z*)-adapted state, the cell-DISCO[21] system was used during incubation with 75 ms light pulses ($\lambda = 370$ nm) every 15 s. Each concentration was tested in duplicate, and each experiment was repeated independently at least four times. 72 h after stimulation, cells were washed with phosphate buffered saline (PBS, 100 μL/well) and stained with propidium iodide (1.0 μg/mL in PBS; 50 μL/well) for apoptosis. After light-protected incubation at 37 °C for 30 min, red object counts were determined via fluorescence imaging on a Tecan Spark Cyto (Tecan Group Ltd.) using the red fluorescence channel. In addition, brightfield imaging was carried out to determine confluence. The red object counts were then normalized to the respective confluence of each well. Statistical analysis was performed in GraphPad Prism (version 9.5.1, GraphPad Software). Statistical significance was evaluated over biological repeats using the mean of technical duplicates. Data sets were tested by ANOVA with post hoc Bonferroni's correction for multiple comparisons. *p*-Values < 0.05 were considered as statistically significant.

Acknowledgements

pUAS-mCherry-NLS was a gift from Robert Campbell (Addgene plasmid no. 87695; http://n2t.net/addgene:87695; RRID: Addgene_87695). J.M. thanks the US National Cancer Institute (NCI) for a K99/R00 award (K99CA277358). Open Access funding enabled and organized by Projekt DEAL.

Conflict of Interest

The authors declare no conflict of interest.

Data Availability Statement

The data that support the findings of this study are available in the supplementary material of this article.

Keywords: liver X receptor · photopharmacology · azobenzene · nuclear transcription factors · photohormones

[1] C. Hong, P. Tontonoz, *Nat. Rev. Drug Discovery* **2014**, *13*, 433–444.
[2] D. D. Moore, S. Kato, W. Xie, D. J. Mangelsdorf, D. R. Schmidt, R. Xiao, S. A. Kliewer, *Pharmacol. Rev.* **2006**, *58*, 742–759.
[3] J. J. Repa, S. D. Turley, J.-M. A. Lobaccaro, J. Medina, L. Li, K. Lustig, B. Shan, R. A. Heyman, J. M. Dietschy, D. J. Mangelsdorf, *Science* **2000**, *289*, 1524–1529.
[4] J. M. Lehmann, S. A. Kliewer, L. B. Moore, T. A. Smith-Oliver, B. B. Oliver, J.-L. Su, S. S. Sundseth, D. A. Winegar, D. E. Blanchard, T. A. Spencer, T. M. Willson, *J. Biol. Chem.* **1997**, *272*, 3137–3140.
[5] I. G. Schulman, *FEBS Lett.* **2017**, *591*, 2978–2991.
[6] J. L. Collins, A. M. Fivush, M. A. Watson, C. M. Galardi, M. C. Lewis, L. B. Moore, D. J. Parks, J. G. Wilson, T. K. Tippin, J. G. Binz, K. D. Plunket, D. G. Morgan, E. J. Beaudet, K. D. Whitney, S. A. Kliewer, T. M. Willson, *J. Med. Chem.* **2002**, *45*, 1963–1966.
[7] J. R. Schultz, H. Tu, A. Luk, J. J. Repa, J. C. Medina, L. Li, S. Schwendner, S. Wang, M. Thoolen, D. J. Mangelsdorf, K. D. Lustig, B. Shan, *Genes Dev.* **2000**, *14*, 2831–2838.
[8] J. Wrobel, R. Steffan, S. M. Bowen, R. Magolda, E. Matelan, R. Unwalla, M. Basso, V. Clerin, S. J. Gardell, P. Nambi, E. Quinet, J. I. Reminick, G. P. Vlasuk, S. Wang, I. Feingold, C. Huselton, T. Bonn, M. Farnegardh, T. Hansson, A. G. Nilsson, A. Wilhelmsson, E. Zamaratski, M. J. Evans, *J. Med. Chem.* **2008**, *51*, 7161–7168.
[9] F. Bovenga, C. Sabbà, A. Moschetta, *Cell Metab.* **2015**, *21*, 517–526.
[10] S. Willems, D. Zaienne, D. Merk, *J. Med. Chem.* **2021**, *64*, 9592–9638.
[11] W. Szymański, J. M. Beierle, H. A. V. Kistemaker, W. A. Velema, B. L. Feringa, *Chem. Rev.* **2013**, *113*, 6114–6178.
[12] J. Broichhagen, J. A. Frank, D. Trauner, *Acc. Chem. Res.* **2015**, *48*, 1947–1960.
[13] M. J. Fuchter, *J. Med. Chem.* **2020**, *63*, 11436–11447.
[14] K. Hüll, J. Morstein, D. Trauner, *Chem. Rev.* **2018**, *118*, 10710–10747.
[15] J. Morstein, M. Awale, J.-L. Reymond, D. Trauner, *ACS Cent. Sci.* **2019**, *5*, 607–618.
[16] J. Morstein, J. B. Trads, K. Hinnah, S. Willems, D. M. Barber, M. Trauner, D. Merk, D. Trauner, *Chem. Sci.* **2020**, *11*, 429–434.
[17] K. Tsuchiya, T. Umeno, G. Tsuji, H. Yokoo, M. Tanaka, K. Fukuhara, Y. Demizu, T. Misawa, *Chem. Pharm. Bull.* **2020**, *68*, 398–402.
[18] K. Hinnah, S. Willems, J. Morstein, J. Heering, F. W. W. Hartrampf, J. Broichhagen, P. Leippe, D. Merk, D. Trauner, *J. Med. Chem.* **2020**, *63*, 10908–10920.
[19] S. Willems, J. Morstein, K. Hinnah, D. Trauner, D. Merk, *J. Med. Chem.* **2021**, *64*, 10393–10402.
[20] J. Ewert, L. Heintze, M. Jordà-Redondo, J.-S. von Glasenapp, S. Nonell, G. Bucher, C. Peifer, R. Herges, *J. Am. Chem. Soc.* **2022**, *144*, 15059–15071.
[21] M. Borowiak, W. Nahaboo, M. Reynders, K. Nekolla, P. Jalinot, J. Hasserodt, M. Rehberg, M. Delattre, S. Zahler, A. Vollmar, D. Trauner, O. Thorn-Seshold, *Cell* **2015**, *162*, 403–411.
[22] M. Färnegårdh, T. Bonn, S. Sun, J. Ljunggren, H. Ahola, A. Wilhelmsson, J.-Å. Gustafsson, M. Carlquist, *J. Biol. Chem.* **2003**, *278*, 38821–38828.
[23] Y. Nishiyama, S. Mori, M. Makishima, S. Fujii, H. Kagechika, Y. Hashimoto, M. Ishikawa, *ACS Med. Chem. Lett.* **2018**, *9*, 641–645.
[24] C.-Y. Lin, J.-Å. Gustafsson, *Nat. Rev. Cancer* **2015**, *15*, 216–224.
[25] H. Cao, S. Yu, D. Chen, C. Jing, Z. Wang, R. Ma, S. Liu, J. Ni, J. Feng, J. Wu, *FEBS Open Bio* **2017**, *7*, 35–43.
[26] P. Heitel, J. Achenbach, D. Moser, E. Proschak, D. Merk, *Bioorg. Med. Chem. Lett.* **2017**, *27*, 1193–1198.

© 2023 The Authors. ChemMedChem published by Wiley-VCH GmbH

18607187, 2023, 11, Downloaded from https://chemistry-europe.onlinelibrary.wiley.com/doi/10.1002/cmdc.202200647, Wiley Online Library on [21/03/2024]. See the Terms and Conditions (https://onlinelibrary.wiley.com/terms-and-conditions) on Wiley Online Library for rules of use; OA articles are governed by the applicable Creative Commons License

[27] J. Schmidt, F.-M. Klingler, E. Proschak, D. Steinhilber, M. Schubert-Zsilavecz, D. Merk, *Sci. Rep.* **2015**, *5*, 14782.
[28] M. Moret, M. Helmstädter, F. Grisoni, G. Schneider, D. Merk, *Angew. Chem. Int. Ed.* **2021**, *60*, 19477–19482; *Angew. Chem.* **2021**, *133*, 19626–19632.
[29] D. Flesch, S.-Y. Cheung, J. Schmidt, M. Gabler, P. Heitel, J. Kramer, A. Kaiser, M. Hartmann, M. Lindner, K. Lüddens-Dämgen, J. Heering, C. Lamers, H. Lüddens, M. Wurglics, E. Proschak, M. Schubert-Zsilavecz, D. Merk, *J. Med. Chem.* **2017**, *60*, 7199–7205.
[30] S. Nomura, K. Endo-Umeda, A. Aoyama, M. Makishima, Y. Hashimoto, M. Ishikawa, *ACS Med. Chem. Lett.* **2015**, *6*, 902–907.
[31] W. Zhang, A. W. Lohman, Y. Zhuravlova, X. Lu, M. D. Wiens, H. Hoi, S. Yaganoglu, M. A. Mohr, E. N. Kitova, J. S. Klassen, P. Pantazis, R. J. Thompson, R. E. Campbell, *Nat. Methods* **2017**, *14*, 391–394.

Manuscript received: November 27, 2022
Revised manuscript received: March 4, 2023
Accepted manuscript online: March 10, 2023

© 2023 The Authors. ChemMedChem published by Wiley-VCH GmbH

18607187, 2023, 11, Downloaded from https://chemistry-europe.onlinelibrary.wiley.com/doi/10.1002/cmdc.202200647, Wiley Online Library on [21/03/2024]. See the Terms and Conditions (https://onlinelibrary.wiley.com/terms-and-conditions) on Wiley Online Library for rules of use; OA articles are governed by the applicable Creative Commons License